Cholinergic suppression of hippocampal sharp-wave ripples impairs working memory

Yiyao Zhang[a,1], Liang Cao[b,1], Viktor Varga[a], Miao Jing[c,d], Mursel Karadas[a], Yulong Li[c,d], and György Buzsáki[a,e,f,g,2]

[a]Neuroscience Institute, Langone Medical Center, New York University, New York, NY 10016; [b]Department of Physics, East China Normal University, 200241 Shanghai, China; [c]State Key Laboratory of Membrane Biology, Peking University School of Life Sciences, Peking-Tsinghua Center for Life Sciences, IDG/McGovern Institute for Brain Research at PKU, 100871 Beijing, China; [d]Chinese Institute for Brain Research, 102206 Beijing, China; [e]Department of Neurology, Langone Medical Center, New York University, New York, NY 10016; [f]Department of Neurosurgery, Langone Medical Center, New York University, New York, NY 10016; and [g]Center for Neural Science, New York University, New York, NY 10003

Edited by Terrence J. Sejnowski, Salk Institute for Biological Studies, La Jolla, CA, and approved March 8, 2021 (received for review August 3, 2020)

Learning and memory are assumed to be supported by mechanisms that involve cholinergic transmission and hippocampal theta. Using G protein–coupled receptor-activation–based acetylcholine sensor ($GRAB_{ACh}3.0$) with a fiber-photometric fluorescence readout in mice, we found that cholinergic signaling in the hippocampus increased in parallel with theta/gamma power during walking and REM sleep, while ACh3.0 signal reached a minimum during hippocampal sharp-wave ripples (SPW-R). Unexpectedly, memory performance was impaired in a hippocampus-dependent spontaneous alternation task by selective optogenetic stimulation of medial septal cholinergic neurons when the stimulation was applied in the delay area but not in the central (choice) arm of the maze. Parallel with the decreased performance, optogenetic stimulation decreased the incidence of SPW-Rs. These findings suggest that septo–hippocampal interactions play a task-phase–dependent dual role in the maintenance of memory performance, including not only theta mechanisms but also SPW-Rs.

working memory | theta | sharp-wave ripples | hippocampus | cholinergic

The neurotransmitter acetylcholine is thought to be critical for hippocampus-dependent declarative memories (1, 2). Reduction in cholinergic neurotransmission, either in Alzheimer's disease or in experiments with cholinergic antagonists, such as scopolamine, impairs memory function (3–8). Acetylcholine may bring about its beneficial effects on memory encoding by enhancing theta rhythm oscillations, decreasing recurrent excitation, and increasing synaptic plasticity (9–11). Conversely, drugs which activate cholinergic receptors enhance learning and, therefore, are a neuropharmacological target for the treatment of memory deficits in Alzheimer's disease (5, 12, 13).

The contribution of cholinergic mechanisms in the acquisition of long-term memories and the role of the hippocampal–entorhinal–cortical interactions are well supported by experimental data (5, 12, 13). In addition, working memory or "short-term" memory is also supported by the hippocampal–entorhinal–prefrontal cortex (14–16). Working memory in humans is postulated to be a conscious process to "keep things in mind" transiently (16). In rodents, matching to sample task, spontaneous alternation between reward locations, and the radial maze task have been suggested to function as a homolog of working memory ["working memory like" (17)].

Cholinergic activity is a critical requirement for working memory (18, 19) and for sustaining theta oscillations (10, 20–22). In support of this contention, theta–gamma coupling and gamma power are significantly higher in the choice arm of the maze, compared with those in the side arms where working memory is no longer needed for correct performance (23–26). It has long been hypothesized that working memory is maintained by persistent firing of neurons, which keep the presented items in a transient store in the prefrontal cortex and hippocampal–entorhinal system (27–31), although the exact mechanisms are debated (32–37). An alternative hypothesis holds that items of working memory are stored in theta-nested gamma cycles (38). Common in these models of working memory is the need for an active, cholinergic system–dependent mechanism (39–41). However, in spontaneous alternation tasks, the animals are not moving continuously during the delay, and theta oscillations are not sustained either. During the immobility epochs, theta is replaced by intermittent sharp-wave ripples (SPW-R), yet memory performance does not deteriorate. On the contrary, artificial blockade of SPW-Rs can impair memory performance (42, 43), and prolongation of SPW-Rs improves performance (44). Under the cholinergic hypothesis of working memory, such a result is unexpected.

To address the relationship between cholinergic/theta versus SPW-R mechanism in spontaneous alternation, we used a G protein–coupled receptor-activation–based acetylcholine sensor ($GRAB_{ACh}3.0$) (45) to monitor acetylcholine (ACh) activity during memory performance in mice. In addition, we optogenetically enhanced cholinergic tone, which suppresses SPW-Rs by a different mechanism than electrically or optogenetically induced silencing of neurons in the hippocampus (43, 44). We show that cholinergic signaling in the hippocampus increases in parallel with theta power/score during walking and rapid eye movement (REM) sleep and reaches a transient minimum during SPW-Rs. Selective optogenetic stimulation of medial septal cholinergic neurons decreased the incidence of SPW-Rs during non-REM sleep (46–48), as well as during the delay epoch of a working memory task and impaired memory performance. These findings demonstrate that memory performance is supported by complementary theta and SPW-R mechanisms.

Significance

Theta oscillations supported by the medial septum are believed to be a critical mechanism for learning and memory. We report that, in addition to theta oscillations, hippocampal SPW-Rs are important. Enhanced cholinergic activation in the hippocampus during the delay between choices in a spontaneous alternation task abolished SPW-Rs and impaired choice performance in mice. Our findings also demonstrate that the outcome of optogenetic manipulation of a key neurotransmitter, acetylcholine (ACh), depends on the state of the brain at the time of the perturbation.

Author contributions: Y.Z. and G.B. designed research; Y.Z. and V.V. performed research; M.J., M.K., and Y.L. contributed new reagents/analytic tools; Y.Z. and L.C. analyzed data; and G.B. wrote the paper.

The authors declare no competing interest.

This article is a PNAS Direct Submission.

[1]Y.Z. and L.C. contributed equally to this work.

[2]To whom correspondence may be addressed. Email: gyorgy.buzsaki@nyulangone.org.

This article contains supporting information online at https://www.pnas.org/lookup/suppl/doi:10.1073/pnas.2016432118/-/DCSupplemental.

Published April 8, 2021.

Results

We first examined the fluctuation of cholinergic signaling in the hippocampus during behavior, using a $GRAB_{ACh}3.0$ (ACh3.0, for short) sensor that allows sensitive monitoring of acetylcholine dynamics at high temporal resolution (45). The adeno-associated viruses (AAV) with human-synapsin promoter (hsyn) encoding ACh3.0 was injected into the dorsal hippocampus in one hemisphere of ChAT-Cre ($n = 7$) and C57/B6 mice ($n = 3$). Three weeks after virus injection of the target CA1 neurons, an optic fiber (200 or 400 μm) was implanted above the pyramidal cell layer of these mice (Figs. 1 and 2*A*). At the same time, a multishank silicon probe was also implanted 200 to 300 μm posterior to the optic fiber in CA1 area (Fig. 1*A*).

Cholinergic Activity and theta–SPW-R Antagonism. During spontaneous behavior in either the mouse's home cage or on an open platform (50 cm × 50 cm), the optically detected ACh3.0 fluorescent signal fluctuated in parallel with motor activity, increasing during locomotion and decreasing during immobility (Fig. 2 *A* and *B*), while the fluorescent signal of ACh-insensitive ACh3.0-mut sensor did not show a relationship with movement (*SI Appendix*, Fig. S1*A*). To quantify this relationship, we plotted the fluorescence signal as a function of running speed and found a reliable positive correlation (Fig. 2 *B* and *C*; Pearson correlation coefficient $r = 0.61 \pm 0.11$; $P < 0.001$; $n = 14$ sessions in nine mice). When the experiment was repeated after intraperitoneal injection of atropine (25 mg/kg), which is an acetylcholine muscarinic receptor antagonist, the speed versus fluorescence correlation was largely eliminated (Fig. 2 *B* and *C*; Pearson correlation coefficient $r = 0.16 \pm 0.08$, $P < 0.0001$; $n = 9$ sessions in seven mice) and was significantly lower than in drug-free sessions (unpaired t test $P = 5.4 \times 10^{-9} < 0.0001$).

Voluntary motor activity, such as ambulation, is invariably related to the magnitude of theta oscillation (49). As expected, during spontaneous behavior, the power of theta oscillation was reliably correlated with ACh3.0 activity (Fig. 2 *D* and *E*; $R = 0.36 \pm 0.1$, $n = 4$ mice). In addition, the theta score (theta/delta power) versus ACh3.0 signal correlation also persisted during REM sleep ($r = 0.44 \pm 0.13$, $n = 4$ mice), when motor activity was at its minimum among all brain states (50). At the onset of non-REM–REM transitions, ACh3.0 fluorescent activity increased and fluctuated as a function of the regularity and amplitude of theta waves (Fig. 2*F*). Comparisons of the REM-fluorescent values with equal duration pre-REM and post-REM epochs of non-REM sleep showed significant differences, parallel with the theta score changes (Fig. 2*G*). These findings confirm previous observations, using less sensitive methods to monitor cholinergic activity (51–54), about the relationship between cholinergic tone and behavioral state (waking, non-REM, and REM) and also demonstrate that speed modulation of the ACh3.0 measures acetylcholine release in the hippocampus in vivo.

The ACh3.0 signal displayed a quasi-rhythmicity at 0.01 to 0.1 Hz (ultra-slow oscillation) during non-REM. The troughs of the ACh3.0 signal cycles coincided with the occurrence of SPW-Rs, after which the ACh3.0 signal rose again (Fig. 3 *A* and *B*). To quantify the time course of ACh3.0 signal–SPW-R occurrence relationship, we used two methods. First, we cross-correlated the peak power timing of each SPW-R (a discrete measure) to the surrounding changes of cholinergic signal and found a significant negative correlation between these variables (Fig. 3 *B* and *C*). Second, we calculated the cross-correlation between the ACh3.0 signal and the integrated power of the ripple band–filtered local field potential (LFP) (140 to 250 Hz) during non-REM sleep in 0.5 s epochs. The maximum power of SPW-R coincided with the minimum of the fluorescence signal in a ∼10 s wide time window (Fig. 3*D*). In contrast, when ACh3.0 signal was correlated with the integrated power of either slow (30 to 80 Hz) or fast (80 to 120 Hz) gamma oscillations during theta-associated behaviors, the gamma power positively cofluctuated with the ACh3.0 signal (Fig. 3*D*). Overall, these findings not only show that theta/gamma and SPW-Rs are competing and mutually exclusive network patterns (55) but also demonstrate that septo–hippocampal cholinergic signaling is an important contributor to this antagonistic relationship.

Prior to the behavioral experiments, we tested the effectiveness of cholinergic activation in the hippocampus by optogenetic stimulation of medial septum in ChAT-Cre transgenic mice ($n = 2$), injected with a virus (AAV-Hsyn-DIO-ChR2) and implanted with the ACh3.0 sensor probe in the dorsal hippocampus (Fig. 1*A*). Optogenetic stimulation of medial septum cholinergic neurons during non-REM sleep induced an increase ($5.47 \pm 2\%$; $P = 0.0004$, paired t test, $n = 7$ trials in a single mouse) in fluorescence that returned to the baseline after > 10 s (Fig. 3*E*), comparable to the magnitude of change between immobility and locomotion. In contrast, the same optogenetic stimulation during running induced only a minor change in the signal (from $1.99 \pm 1.7\%$ to $2.41 \pm 1.41\%$, paired t test: $P = 0.09$, $n = 25$ trials in two mice), due likely to the already high release of acetylcholine during locomotion (48). As reported before, optogenetic stimulation of cholinergic neurons in the medial septum markedly reduced the occurrence of SPW-Rs (Fig. 3*F*) (46–48).

To probe for potential nonspecific, heat-induced effects of light stimulation (56), 10 s long light pulses (473 nm; ∼5 mW; as in the behavioral experiments below) were used in a ChAT-Cre mouse. The light pulses induced ∼0.3 °C change, measured immediately next to the optic fiber in the medial septum (*SI Appendix*, Fig. S1 *B–D*), but this stimulation did not affect ACh3.0 signaling (from -1.03 ± 2.64 versus $-1.13 \pm 2.67\%$, paired t test, $P = 0.2633$, $n = 85$ trials in three mice).

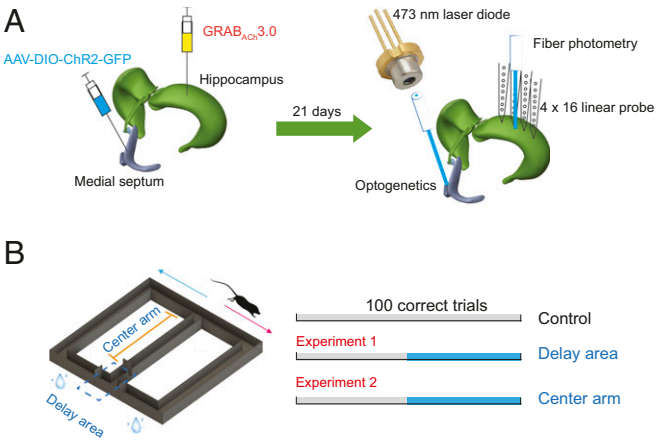

Fig. 1. Experimental design. (*A*) $GRAB_{ACh}3.0$ (ACh3.0) virus was injected in hippocampal CA1 area (ACh fiberphotometry) in ChAT-Cre transgenic and C57/B6 mice, and AAV-DIO-ChR2-GFP was injected in medial septum of ChAT-Cre transgenic mice (optogenetics). After 21 d of virus injection, optical fiber was implanted in the medial septum for optogenetic activation of cholinergic neurons. Optical fiber for photometric measurement and silicon probe for electrophysiological recording were implanted in the hippocampal CA1 region. (*B*) Mice were trained to learn a hippocampus-dependent figure-eight–maze task. They were rewarded each time they reached the end of side maze arms in the correct task sequence (center-left-center-right-center, and so on). Between choices, they were confined in the start (delay) area for 10 s. Optogenetic stimulation was administered in the delay area or center arm.

Optogenetic Enhancement of Cholinergic Activity during Memory Delay Decreases Performance. Memory performance in the spontaneous alternation task depends on the duration of the delay between choices. This task is hippocampus dependent and is often portrayed as analogous to working memory in humans (16,

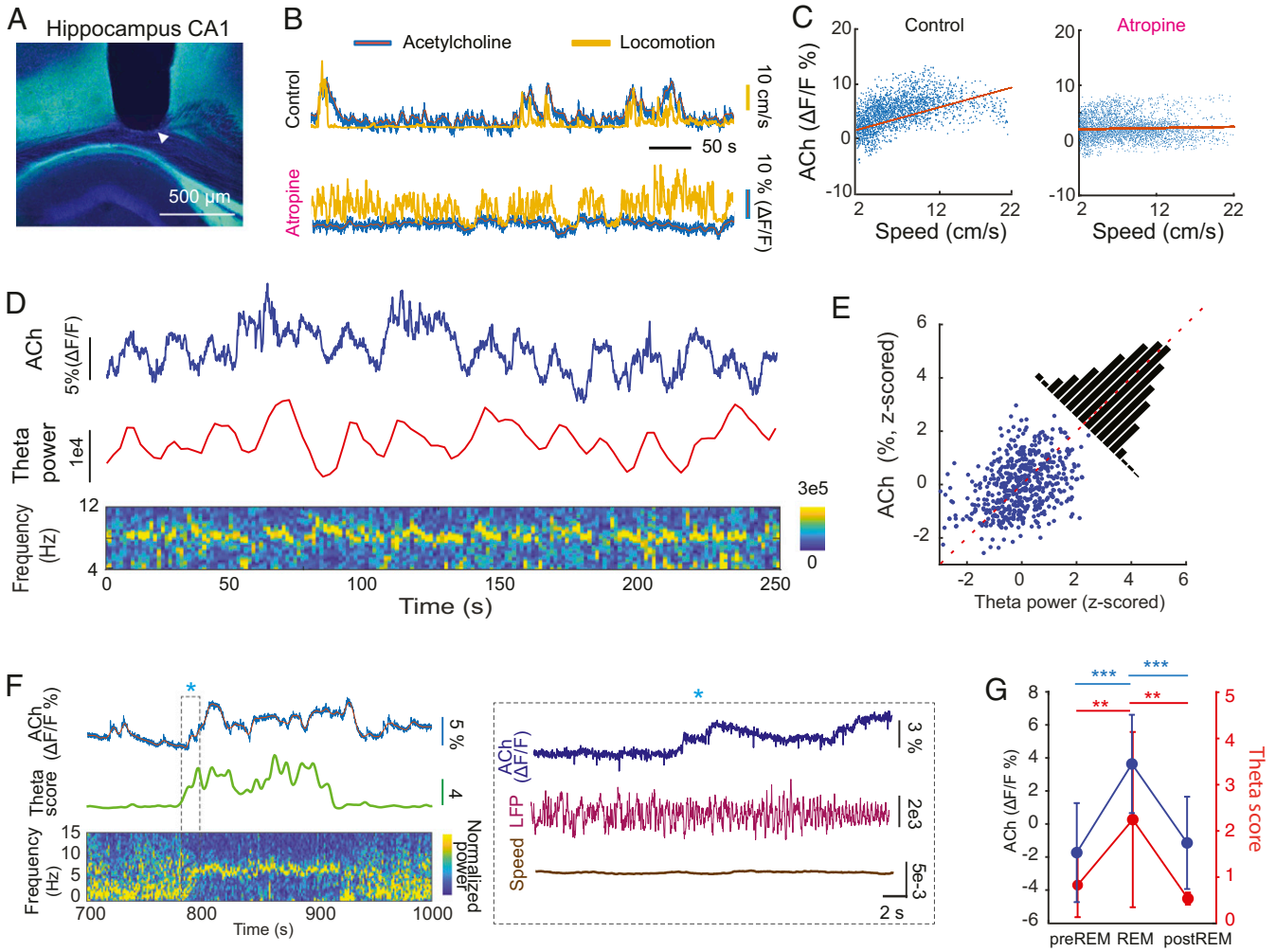

Fig. 2. Behavior dependence of cholinergic activation in the hippocampus. (*A*) Track of optic fiber above the CA1 region of the hippocampus (tip is marked by white arrowhead). The ACh3.0 sensor was expressed in the hippocampal neurons by AAVs to allow detection of ACh dynamics in vivo. (*B*) An example ACh3.0 fluorescence signal, measured by fiber photometry, and movement recorded during spontaneous activity before (*Top*) and after intraperitoneal atropine injection (25 mg/kg; *Bottom*). (*C*, *Left*) The correlation between ACh3.0 fluorescence signal and speed of locomotion (Pearson correlation coefficient $r = 0.64$, $P = 0$). (*C*, *Right*) The correlation between ACh3.0 signal and speed of locomotion after atropine system injection ($r = 0.06$, $P = 0$). (*D*) The relationship between ACh3.0 signal and integrated theta oscillation power during spontaneous behavior. (*D*, *Bottom*) Time-resolved power spectrogram of hippocampal LFP. (*E*) The correlation between ACh3.0 fluorescence signal and theta power ($r = 0.361$, $P = 4.55 \times 10^{-18}$). (*F*) The relationship between ACh3.0 signal and theta oscillation score (*Materials and Methods*) during REM sleep. The transition between non-REM and REM (asterisk) is shown at a higher time resolution in the *Right*. (*G*) ACh3.0 signal (*Left y* axis) increases during theta-rich REM sleep (theta score; *Right y* axis) compared to equal lengths of non-REM epochs before and after REM sleep. ($n = 18$ REM episodes in four mice; one-way ANOVA; theta score: $P = 0.0007$, ACh: $P < 0.0001$; Holm–Sadik's multiple comparison test. Theta score: pre-REM (0.83 ± 0.69), REM (2.25 ± 1.90), and post-REM (0.54 ± 0.13), ACh3.0 fluorescent value: pre-REM (−1.73 ± 3%), REM (3.64 ± 3%), post-REM (1.15 ± 2.79%). $^{**}P < 0.01$; $^{***}P < 0.001$.

17, 34). Since working memory is suggested to depend on cholinergic activity and associated theta oscillations (18, 19), we wondered whether boosting of medial septum cholinergic activity affects memory performance.

To examine the relationship between memory, behavior, electrophysiological activity, and cholinergic activity, we first examined cholinergic activation during spatial alternation behavior in a figure-eight maze (Fig. 1*B*). Two C57/B6 and two ChAT-ChR2 mice were injected with ACh3.0 in dorsal CA1 region (Fig. 1*A*). The cholinergic signal was highest in the central (choice) arm, associated with increased theta/gamma power (10, 20, 21), and was lowest in the delay area (Fig. 4*A*). In the delay area, mice often showed frequent head turns and rearing on the walls of the start area during the first part of the delay. During the later part of delay, the overt motor activity decreased, which we quantified by measuring head movements ("speed" orange line; Fig. 4 *A*, *ii*). The decreasing motor activity during the delay, which was more apparent on trials of the second part of the session, was reflected by a commensurate decrease of the ACh3.0 signal (Fig. 4*A*). Parallel with the cholinergic and behavioral changes, the incidence of SPW-Rs increased (Fig. 4*B*). Optogenetic activation of medial septal cholinergic neurons in the delay area increased the ACh3.0 signal (from −1.9 ± 2.8 to 1.47 ± 1.48%, $n = 44$ trials, paired t test, $P = 5.58 \times 10^{-8}$; single mouse).

Since the cholinergic signal in the hippocampus decreased during the delay in the alternation task, we next tested how increasing ACh release in the hippocampus affects choice behavior and SPW-Rs. Six ChAT-ChR2 transgenic mice were trained in the figure-eight maze to run for 100 correct trials in a daily session to obtain water reward (Figs. 1*B* and 5*A*). Between left and right arm choices, the mouse was confined to the delay area for 10 s. After initial training (7 d), mice were implanted with an optic fiber

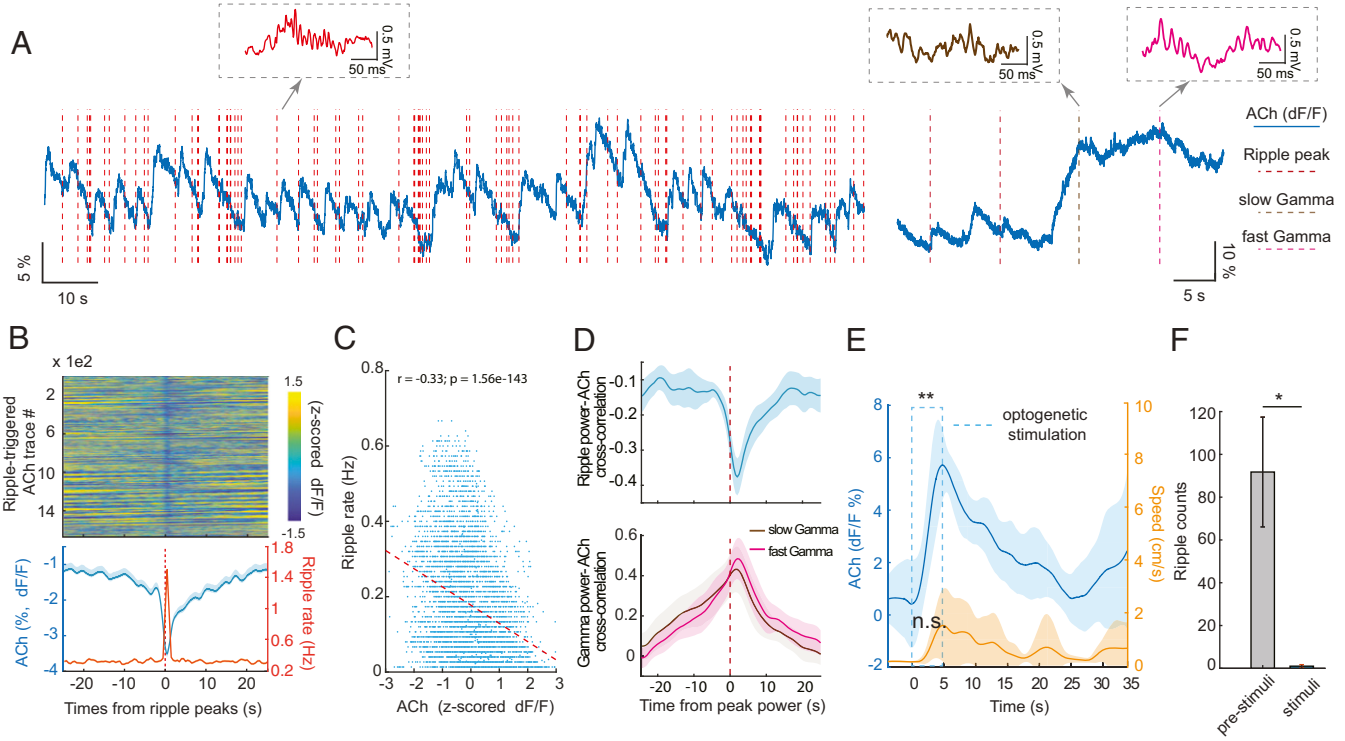

Fig. 3. SPW-Rs occur when hippocampal cholinergic activation transiently decreases during slow wave sleep (SWS). (*A*) Example traces of ACh3.0 signal fluctuation (blue line) and SPW-R occurrence (red vertical dashed lines) during non-REM (*Left*) and non-REM–waking transient (*Right*). Examples of SPW-R, slow (brown) and fast gamma epochs (purple), extracted from the simultaneously recorded LFP, are shown as insets. (*B*, *Top*) Color-coded, normalized change of ACh3.0 signal surrounding SPW-Rs during non-REM sleep (n > 1,600 SPW-Rs from 4 non-REM sessions, single mouse). (*B*, *Bottom*) Mean change (± SEM) of ACh3.0 (blue) and ripple rate (orange) centered on the peak power timing of ripple events. (*C*) The relationship between ACh3.0 signal and ripple rate (n = 10 sessions in four mice). (*D*, *Top*) Cross-correlations between ACh3.0 signal and continuous ripple-band–filtered (140 to 250 Hz) LFP power in 0.5 s epochs (from six non-REM sleep sessions in three mice). (*D*, *Bottom*) Cross-correlation between ACh3.0 signal and continuous gamma-band–filtered (30 to 80 Hz slow gamma and 80 to 120 Hz fast gamma) LFP power (from six waking sessions in four mice). (*E*) Time course of optogenetically induced ACh3.0 signal during sleep. Medial septum was optogenetically stimulated by 5 s long pulses during non-REM sleep. ACh3.0 signal increased significantly during stimulation (0.48 ± 1.4% prior to stimulation; 5.95 ± 0. 83% by the end of stimulation; $^{**}P = 0.004$, two-tail paired test, n = 7 trials). Movement (*Right y* axis) occurred on some trials, but overall, it did not change significantly during stimulation ($P = 0.052$, two-tail paired t test). (*F*) Optogenetic stimulation of cholinergic medial septal neurons suppressed SPW-R occurrence during non-REM sleep (paired t test: $^{*}P = 0.04$, n = 4 mice). $^{*}P < 0.05$.

(100 μm diameter) to selectively stimulate medial septal cholinergic neurons optogenetically (46, 48) and recording silicon probes in the hippocampus (Fig. 1*A*).

We first examined the relationship between choice performance and the incidence of SPW-Rs in delay area in CONTROL sessions. The rate of SPW-Rs was calculated from epochs when the mouse sat immobile (speed <3 cm/s). The incidence of SPW-Rs increased monotonically within CONTROL sessions without medial septum stimulation (n = 3 to 5 consecutive daily sessions; Fig. 5 *A*–*C*; total of 21 sessions in six mice). After two rest days, another four to five daily sessions were performed. In these sessions, the first 50 trials served as control trials (first half of session), followed by another 50 trials (second half of session) with optogenetic stimulation of medial septal cholinergic neurons (OPTO sessions; total of 25 sessions in six mice). In contrast to the CONTROL sessions, the rate of SPW-Rs remained low throughout the OPTO sessions, and the rate of SPW-Rs in the stimulated (second) half of the session was significantly lower than in the comparable second half of CONTROL sessions (Fig. 5 *B* and *C*). At the same time, during OPTO trials, choice performance decreased relative to both the first (no stimulation) part of the session and the comparable second half of CONTROL sessions (Fig. 5 *D* and *E*). The results cannot be explained by OPTO stimulation–induced behavioral change since the percent of time spent immobile in the delay area in trials 51 to 100 was not affected by the stimulation (Control = 33.2 ± 16.88%, OPTO = 39.1 ± 13.57%; unpaired t test, P = 0.23).

Three of the six mice were further tested for an additional 8 to 10 d after 2 d of rest. The first 3 to 5 d (total of 13 sessions; three mice) were nonstimulation CONTROL sessions. In the next 5 d, medial septum optogenetic stimulation protocol was resumed (total of 15 sessions, three mice). However, this time optogenetic stimulation (OPTO) was applied while the mouse ran in the central arm of the maze. Optogenetic stimulation in the central arm did not affect memory performance (Fig. 5 *D* and *E*). The incidence of SPW-Rs in the delay areas was slightly reduced (Fig. 5*B*, $P > 0.05$), possibly due to the long-lasting aftereffect of optogenetic stimulation on cholinergic activity (Fig. 3*D*). The rate of SPW-Rs during trials 51 to 100 of the OPTO session in the center arm was significantly higher than during OPTO stimulation in the delay area (Fig. 5*B*, P = 0.0034 < 0.01). The percent of time spent immobile in the delay area in trials 51 to 100 was not affected by the stimulation (Control = 11.2 ± 0.2%, OPTO = 8.77 ± 0.03%; unpaired t test, P = 0.21).

Discussion

Our findings demonstrate that the outcome of optogenetic manipulation of a key neurotransmitter, ACh, depends on the state of the brain at the time of the perturbation and suggest that memory in the delayed spontaneous alternation task is supported by both theta and SPW-R mechanisms.

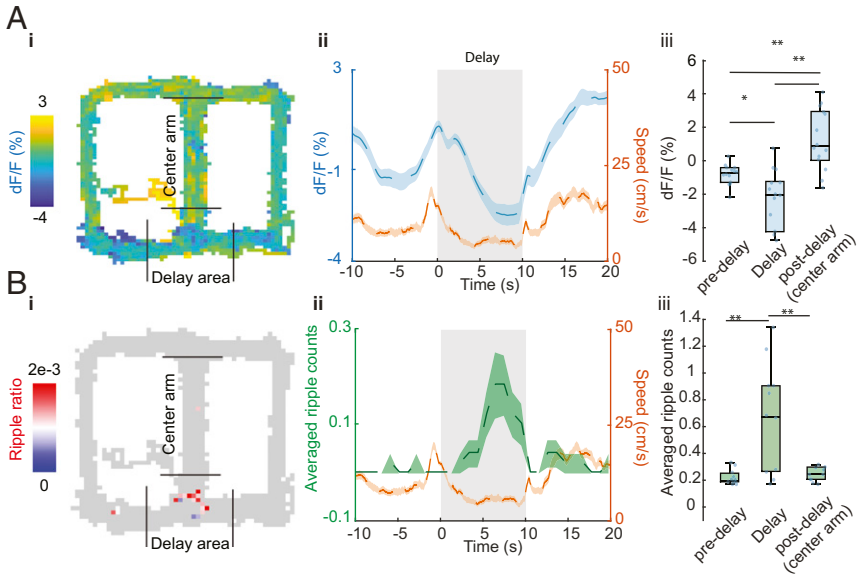

Fig. 4. The relationship between ACh3.0 signal and SPW-Rs during spontaneous alternation behavior. (*A*) ACh3.0 fluorescence change during figure-eight–maze task. (i: ACh3.0 fluorescence signal on the maze, ii: Running in central and side arms and staying in the delay area show differential ACh signal modulation. $n = 50$ trials in an example session; mean ± SEM, iii: Group statistic of ACh3.0 signal for predelay area (−0.12 ± 0.64%), delay area (−2.42 ± 3.62%), and postdelay area (2.1 ± 1.9%). $n = 14$ sessions from four mice, $P = 0.0006$, one-way ANOVA, post hoc $^{*}P < 0.05$; $^{**}P < 0.01$; Holm–Sidak's multiple comparison test. (*B*) SPW-Rs distribution during T-maze task. i: Example session of SPW-Rs distribution on the maze, ripple ratio: averaged ripple counts per bin (1 cm^2). ii: Peri-delay area averaged ripple counts and locomotion results change during maze task. Speed signal is the same as in *A*. $n = 50$ trials. iii: Group statistics of average ripple counts in the predelay area (0.05 ± 0.06), delay area (0.56 ± 0.45), and postdelay area (0.10 ± 0.09). $n = 11$ sessions from 3 mice, $P = 0.0022$, one-way ANOVA, post hoc $^{**}P < 0.01$; Holm–Sidak's multiple comparison test.

Working memory is usually defined as an "effortful" conscious operation (16) that depends on the brain's "attentional" system (57). Human studies demonstrate that "keeping items in mind" is associated with sustained theta oscillations in the hippocampal system and prefrontal areas ("midline theta") (58, 59). Based on neuronal recordings from single neurons in the prefrontal cortex in primates, it has been suggested that the cellular mechanism of working memory is persistent firing of a subset of neurons throughout the time window of working memory. Ample experimental evidence supports the critical role of Ach in both persistent firing (10) and theta oscillations (8, 9, 41, 60, 61). However, when the delay between encoding and using that information is long, it is unlikely that persistent firing alone can support the maintenance of the trace. It has been suggested that working memory recruits episodic memory mechanisms at longer delays, supported by the hippocampus (34). This suggested division, based on the duration of delay, may explain the contribution of SPW-Rs in the figure-eight spatial alternation task.

Previous experiments in rodents have offered an alternative mechanism underlying working memory, at least as it applied to alternation and matching-to-sample tasks. Recordings in the medial prefrontal cortex have shown that persistently firing neurons during the delay period were mainly inhibitory interneurons (62). Pyramidal neurons, instead of displaying sustained firing, form chains of sequentially active assemblies, in which each pyramidal neuron is active only for approximately 1 s (62). Similarly, hippocampal neurons during the delay form sequentially active neuronal trajectories, unique to the future action selection (63). Hippocampal theta oscillations have been proposed as the mechanism for the chaining neuronal activity, and it has been tacitly assumed that when an animal is confined in the delay area between choices, sustained theta oscillation can support neuronal chaining (64). In further support of the importance of theta rhythm, drug-induced blockade of local activity or temperature decrease in the medial septal area reduce or alter theta oscillations and impair memory performance (8, 9, 41, 60, 61, 65). On the other hand, several observations indicate that rodents often remain still, associated with hippocampal SPW-Rs, in the delay area of a spontaneous alternation task (55). Importantly, when SPW-Rs are perturbed or prolonged by artificial means, working memory is impaired or improved, respectively (43, 44). However, the relationship between theta and SPW-R mechanisms and the postulated exclusive role of cholinergic signaling have remained to be explored.

In our experiments, we examined the effect of sustained cholinergic activation on memory performance. In control trials, SPW-Rs increased steadily over trials. In the delay area, fiber photometric detection of ACh3.0 activity fluctuated and sudden drops in ACh3.0 signal coincided with the occurrence of SPW-Rs. When optogenetic stimulation of medial septal cholinergic neurons was applied in the delay area, the occurrence of SPW-Rs was reduced, accompanied by deterioration of memory performance. In contrast, when the same optogenetic stimulation was performed in the central arm where no SPW-Rs were observed, memory was not affected. Furthermore, transient peaks of ACh3.0 activity coincided with increased power of both slow and fast gamma oscillations, demonstrating that despite the multiple similarities between SPW-Rs and gamma oscillations (55), they are fundamentally different and antagonistic patterns. Related to the present observations, spatial memory in a radial arm maze was abolished when tetracaine was injected into the medial septum during the learning phase, but septal inactivation during the delay epoch did not affect choice accuracy of not yet visited arms (66), presumably allowing SPW-Rs to sustain information about choices already made. SPW-Rs possibly potentiated the relevant synapses that carried information about the items to be remembered. A new picture that emerges from the above studies is that theta oscillations and SPW-Rs play a complementary role in working memory. Yet, we also acknowledge the remote possibility that increased activity of cholinergic neurons by optogenetic stimulation might bring

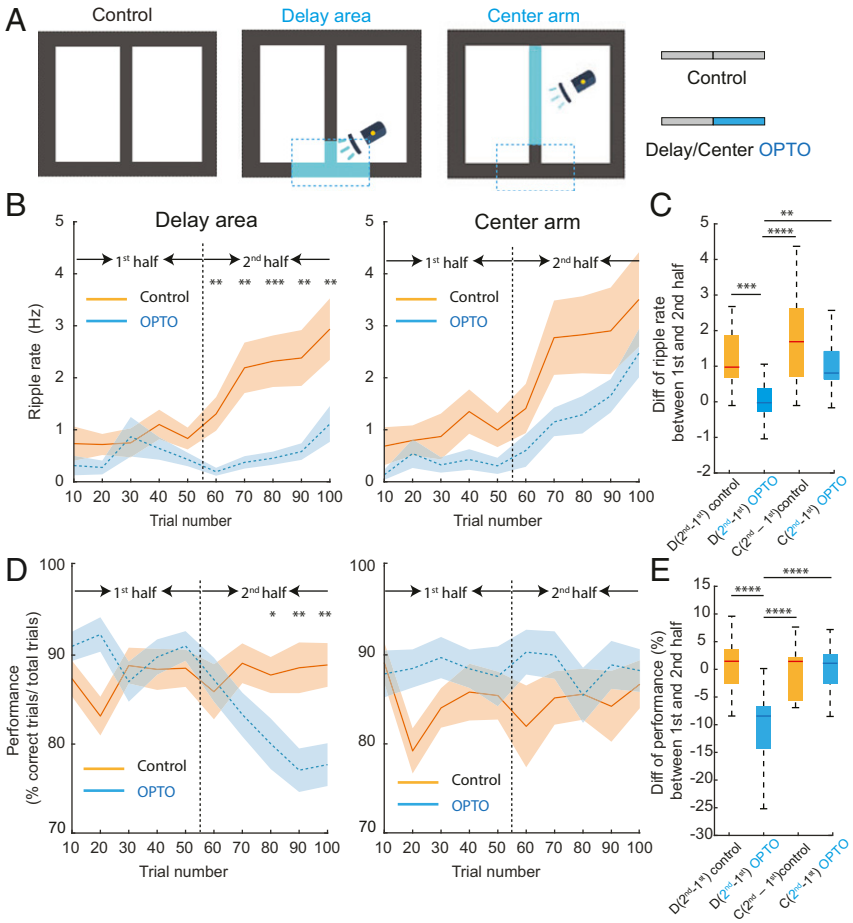

Fig. 5. Cholinergic activation during delay area between choices suppresses SPW-Rs and impairs spatial working memory but not activation during center arm. (*A*) An illustration of task protocol (100 correct trials total). Control: no stimulation sessions, Delay sti: cholinergic stimulation (OPTO) during the last 50 trials in delay area (Blue) in delay sessions. Center sti: cholinergic stimulation during last 50 trials in the center arm (OPTO). (*B*) SPW-R rate (ripple rate) during the first half (1 to 50 correct trials) and second half (51 to 100 correct trials in no stimulation (Control) and optogenetic stimulation (OPTO) sessions in the delay area (*Left*) or center arm (*Right*). Averages across all sessions (mean ± SEM). Note the steady increase in SPW-R rate during Control sessions and decreased SPW-R during OPTO stimulation in the delay area and continued increase in session with OPTO stimulation in the central arm. Control versus OPTO: Unpaired *t* test, $*P < 0.05$; $**P < 0.01$; $***P < 0.001$. (*C*) Comparison of SPW-R rate difference between the first and second halves of trials in Control and OPTO stimulation sessions in the delay area (D) or central arm (C). One-way ANOVA: $P < 0.0001$, post hoc Holm–Sidak's multiple comparison tests: $*P < 0.05$; $**P < 0.01$; $***P < 0.001$, $****P < 0.0001$. D(second – first)control = 1.39 ± 1.22 Hz, D(second – first)OPTO = –0.0009 ± 0.68 Hz, C(second – first)control = 1.74 ± 1.45 Hz, C(second – first)OPTO = 1.09 ± 0.85 Hz, mean ± SD. (*D*) Behavioral performance during the first half (1 to 50 correct trials) and second half (51 to 100 correct trials) in no stimulation (Control) and optogenetic stimulation (OPTO) sessions in the delay area (*Left*) or center arm (*Right*). Averages across all sessions and mice (mean ± SEM). Note the deterioration of memory performance during OPTO stimulation in the delay area. Control versus OPTO: Unpaired *t* test, $*P < 0.05$; $**P < 0.01$. (*E*) Comparison of behavioral performance difference between the first and second halves of trials in Control and OPTO stimulation sessions in the delay area (D) or central arm (C). One-way ANOVA: $P < 0.0001$, post hoc Holm–Sidak's multiple comparison test: $*P < 0.05$; $**P < 0.01$; $***P < 0.001$, $****P < 0.0001$. D(second – first)control = 0.63 ± 5.23%, D(second – first)OPTO = –10 ± 6.91%, C(second – first)control = –0.10 ± 4.62%, C(second – first)OPTO = 0.16 ± 4.17%, mean ± SD.

about deleterious effects via hitherto unidentified mechanisms, independent of their SPW-R-suppressing effect.

Whether and how observations in rodents performing a spontaneous alternation task relates to working memory remains to be clarified. Deep electrode and subdural grid recordings in human subjects have shown that SPW-Rs emerge prior to recall, and both the incidence and the efficacy of coupling between hippocampal SPW-Rs and relevant neocortical sites correlate with memory performance (67, 68). Similarly, magnetoencephalography recordings in healthy humans revealed the occurrence of ripples prior to correct recall (69). The possible complementary contribution of both theta/gamma and SPW-Rs mechanisms to working memory poses new questions. While cholinergic activity and cholinomimetic drugs are generally assumed to improve attention and working memory, our findings imply that the timing of drug effects is crucial, and their effect is biased by ongoing brain activity. Our experiments support previous observation in humans that increasing the cholinergic tone during non-REM sleep or quiet wakefulness can be detrimental to memory (70) and a likely mechanism in suppressing SPW-Rs. Furthermore, neuroprotectants that effectively reduced neuronal damage when applied during sleep were ineffective when administered during waking hours (71). Overall, our findings demonstrate that alternating high and low tones of cholinergic activity and associated interleaving theta and SPW-R patterns are both important for working memory with longer delays, possibly acting on its different aspects.

Materials and Methods

Surgical Procedure. All experiments were approved by the Institutional Animal Care and Use Committee at New York University Langone Medical Center. General anesthesia was induced with isoflurane inhalation. For survival surgery (injection of virus or implantation of probes and optical fibers), anesthesia was maintained by isoflurane through a mask mounted on the stereotaxic apparatus. Body temperature was kept constant with a heating pad (37 °C).

Virus Injection. The skull was exposed under antiseptic conditions using local anesthesia with bupivacaine/lidocaine, and holes were drilled above the medial septum and hippocampus CA1 [Medial septum: anteroposterior (AP) + (0.7 to 0.9 mm), midline insertion at 0° angle. Hippocampus: AP −2.3 mm, ML ± 2.00 mm]. A glass pipette (30 to 50 μm tip) connected to a Nanoject II/Nanoliter 2000 microinjector (Drummond Scientific Co. or WPI Inc.) was used to inject 0.05 to 0.07 μL of virus solution at three different depths between 3.2 and 4.0 mm (midline, 0 angle) of Medial septum, and 0.1 μL of virus solution at 1.2 and 1.5 mm depths of Hippocampal CA1, over 15 min. After injection the pipette was removed slowly (0.1 then 0.5 mm steps, 10 min waiting periods between each) and the scalp was sutured.

Silicon Probes and Optical Fiber Implantation. Silicon probes (64 sites, 4 or 5 shank, NeuroNexus) were inserted into hippocampal CA1 area at 1 to 2.5 mm depth. Silicon probes were mounted on a microdrive and progressively lowered into the CA1 pyramidal layer (0.8 to 1.3 mm depth) during post-surgical recovery period (recognized by the presence of ripples and strong spiking). In the MS, a 105 μm diameter optical fiber was implanted at a depth of 3.2 mm. Before surgery, the optic fiber was stripped from the outer layer and connectorized with 1.25 mm ceramic ferrules (extracted from LC connectors; Thorlabs). A pencil-shaped tip was obtained by etching for 30 s in hydrofluoric acid (Sigma) to facilitate the insertion in the brain and increase light scattering.

ACh3.0 Fluorescent Signal and Fiber Photometry. The virus AAV-hSyn-ACh3.0 (Vigene Biosciences Inc) was injected into the dorsal hippocampus, and a 200 (Thorlabs FP200URT, NA = 0.5, n = 6 mice) or 400 μm (Thorlabs FP400URT, NA = 0.5, n = 4 mice) diameter optic fiber was implanted 200 to 300 μm above injection site to collect the emission fluorescent signal from that area. During recording, a 400 Hz square-wave train, driven LED (470 nm, LED driver (LEDD1B), and fiber-coupled LED (M470F3) from Thorlabs) by a signal generator (Rigol DG4062 Arbitrary Waveform Generator) was delivered to excite ACh3.0 sensor. The light power, measured from mono fiberoptic patchcord (FC-MF1.25) tip by PM100D from Thorlabs, in air, was 30∼60 μW. The delivered power to the brain was 80 to 95% of the input power. The light excitation and fluorescence detection is done through a Mini cube with three ports (FMC3-e(460 to 490) F(500 to 550)_S, Doric). The emission light of ACh3.0 signal in dorsal hippocampus traveled back through the same optical fiber and bandpass filtered (500 to 550 nm) in the Minicube and detected by a Femtowatt Silicon Photoreceiver (Newport, 2151). The detected signal passed through a lowpass filter (Model 440 instrumentation Amplifier) at 20 Hz and recorded using a real-time processor (CED power 1401). The ACh 3.0 fluorescent response was obtained using the equation $\Delta F/F = (F - F_0)/F_0$, in which the F_0 is the baseline signal detected by a fifth order polynomial fitting.

Optogenetics Stimulation. Light from a 473 nm diode-pumped solid state laser (Dreamlasers) was collimated with a fiberport (Thorlabs) or delivered by a 473 nm laser diode light source (Fluorescence Module Including Light Source; FLS-475 nm–20 mW; Diffraction Image Phase Sensing Instrument or laser diodes with a built-in monitor photodiode: L473P100; Thorlabs) into a custom patch cord (Thorlabs) connected to the brain-implanted optic fiber. Light intensity was driven by analog modulation of a CED micro1401 mkII data acquisition system (Cambridge Electronic Devices) to generate sinusoidal patterns. For stimulation of MS (n = 10 animals), maximum light intensity (crest of the sine wave or plateau pulse amplitude) was adjusted using a photodiode power sensor coupled to a power meter (S130A and PM30 or S130C and PM100USB; Thorlabs), taking into account the patch-cord-to-fiber coupling (measured before implantation of the fiber), to obtain a maximum of 5 to 10 mW at the tip of the fiber in the brain.

Recording and Data Acquisition. Recordings were conducted using the Intan RHD2000 interface board, sampled at 20 kHz. Amplification and digitization were done on the head stage. For chronic recording, animals were recorded in their home cage during sleep, alert immobility, actively awake (grooming, sniffing, etc.), and/or during the exploration of a different environment (50 × 50 cm open field arena or 56 × 56 figure-eight–maze task. For all behavioral experiments, position was tracked with the OptiTrack camera system. Infrared reflective markers were mounted in unique positions on each animals' head stage and imaged simultaneously by six cameras (Flex 3) placed above the behavioral apparatus. Calibration across cameras allowed for the three-dimensional reconstruction of the animals' head position and head orientation to within 1 mm (average displacement error = 0.70 ± 1.5 mm) at 100 Hz. Position data were analyzed and segmented using a custom MATLAB software suite.

SPW-R Detection and Ripple Rate. The LFP from a selected channel (largest ripple power) was 140 to 250 Hz bandpass filtered by a fourth order Butterworth filter, and then the Hilbert transform were applied to filtered LFP to get ripple band amplitude. Candidate events was detected by choosing the periods that the ripple band amplitude is 2 SD above the mean, peak amplitudes >5 SD, and duration between 30 and 200 ms. After that, SPW-Rs were manually selected from candidate events by looking at the raw LFPs from neighboring channels. Ripple rate is determined using 0.5 s (Fig. 3*B*) or 3 s (Fig. 3*C*) time window and smoothed by moving average of 1.5 or 9 s.

LFP Analysis. The 20 kHz recorded raw data were low-pass filtered by a sinc filter with a 450 Hz cutoff band and then downsampled to 1,250 Hz to get the LFP. The power spectrogram was calculated using short-time Fourier transform. For delta, theta, slow gamma, fast gamma, ripple power analysis, the LFP was bandpass filtered by 0.5 to 4 Hz, 5 to 10 Hz, 30 to 80 Hz, 80 to 120 Hz, and 140 to 250 Hz, respectively. The band powers were calculated using Chronux multitaper spectrum methods and smoothed with 1-s moving mean window. Theta score is defined as the ratio of power in theta band and delta band). The correlation between LFP power and ACh3.0 signal are measured as Pearson correlation coefficient. The Cross correlations between ACh3.0 signal and Gamma power (slow and fast), ripple power was generated from normalized data of each session.

Histology. Mice were deeply anesthetized with overdosed urethane and perfused transcardially by saline followed either by 4% paraformaldehyde (PFA) or by the Sloviter protocol (i.e., 2% (wt/vol) PFA in acetate buffer (pH 6.5) for 3 min followed by 2% (wt/vol) PFA in borate buffer (pH 8.5) for 40 min). After perfusion, brains were removed and stored in fixative solution overnight. Next, 60 μm sections were prepared on a vibrotome (Leica). Then, sections were washed in 0.1 M phosphate buffer (PB), cryoprotected overnight in 30% (wt/vol) sucrose dissolved in 0.1 M PB, and freeze–thawed in aluminum foil boats over liquid nitrogen to enhance penetration of the antisera. Next, after several changes of PB, the sections were transferred into Tris-buffered saline (TBS, pH 7.4). All of the following washes and antisera dilutions were carried out in TBS. Sections were incubated in primary antibody solution for two nights at 4 °C. Then, primary serum was washed, followed by incubation in secondary antibody solution for 3 h at room temperature, followed by extensive washing. Finally, sections were mounted on glass slides and covered by Vectashield. Antibodies used were mouse chicken polyclonal anti-green fluorescent protein primary (1:2,000; Life Technologies) and Alexa-488 conjugated goat anti-chicken secondary (1:500). All secondaries were purchased from MilliporeSigma. Sections were examined by an Axioplan-2 microscope (Zeiss). Photomicrographs were taken by an Olympus DP-70 CCD camera (Olympus) on the Zeiss microscope. Adjustments of lookup tables of images were accomplished using Adobe Illustrator (Adobe Systems Inc.).

Data Availability. Digital data have been deposited in https://buzsakilab.nyumc.org/datasets/ZhangY/. All study data are included in the article and/or *SI Appendix*.

ACKNOWLEDGMENTS. We thank Nic Tritsch, Dayu Lin, and members of their laboratories for assistance with fiber photometry and members of the G.B. laboratory for feedback on the manuscript. This work was supported by NIH MH122391, MH107396, U19 NS107616, and U19 NS104590. L.C. was supported by the China Scholar Council Fellowship (CSC201806140122). V.V. was supported by a Marie Sklodowska Curie Actions International Fellowship (707359 - HippAchoMod).

1. G. Buzsáki, Two-stage model of memory trace formation: A role for "noisy" brain states. *Neuroscience* **31**, 551–570 (1989).
2. M. E. Hasselmo, Neuromodulation: Acetylcholine and memory consolidation. *Trends Cogn. Sci.* **3**, 351–359 (1999).
3. A. Atri *et al*., Blockade of central cholinergic receptors impairs new learning and increases proactive interference in a word paired-associate memory task. *Behav. Neurosci.* **118**, 223–236 (2004).
4. J. T. Coyle, D. L. Price, M. R. DeLong, Alzheimer's disease: A disorder of cortical cholinergic innervation. *Science* **219**, 1184–1190 (1983).
5. N. Sitaram, H. Weingartner, J. C. Gillin, Human serial learning: Enhancement with arecholine and choline impairment with scopolamine. *Science* **201**, 274–276 (1978).
6. A. Green *et al*., Muscarinic and nicotinic receptor modulation of object and spatial n-back working memory in humans. *Pharmacol. Biochem. Behav.* **81**, 575–584 (2005).

7. J. G. Bunce, H. R. Sabolek, J. J. Chrobak, Intraseptal infusion of the cholinergic agonist carbachol impairs delayed-non-match-to-sample radial arm maze performance in the rat. *Hippocampus* **14**, 450–459 (2004).
8. S. Leutgeb, S. J. Mizumori, Excitotoxic septal lesions result in spatial memory deficits and altered flexibility of hippocampal single-unit representations. *J. Neurosci.* **19**, 6661–6672 (1999).
9. M. G. Lee, J. J. Chrobak, A. Sik, R. G. Wiley, G. Buzsáki, Hippocampal theta activity following selective lesion of the septal cholinergic system. *Neuroscience* **62**, 1033–1047 (1994).
10. M. E. Hasselmo, The role of acetylcholine in learning and memory. *Curr. Opin. Neurobiol.* **16**, 710–715 (2006).
11. M. E. Hasselmo, J. McGaughy, High acetylcholine levels set circuit dynamics for attention and encoding and low acetylcholine levels set dynamics for consolidation. *Prog. Brain Res.* **145**, 207–231 (2004).
12. J. J. Buccafusco, S. R. Letchworth, M. Bencherif, P. M. Lippiello, Long-lasting cognitive improvement with nicotinic receptor agonists: Mechanisms of pharmacokinetic-pharmacodynamic discordance. *Trends Pharmacol. Sci.* **26**, 352–360 (2005).
13. M. Scarpa, S. Hesse, S. J. Bradley, "M1 muscarinic acetylcholine receptors: A therapeutic strategy for symptomatic and disease-modifying effects in alzheimer's disease?" in *Advances in Pharmacology*, S. J. Enna, Ed. (Elsevier, 2020), 88, pp. 277–310.
14. E. E. Smith, J. Jonides, Storage and executive processes in the frontal lobes. *Science* **283**, 1657–1661 (1999).
15. J. P. Aggleton, P. R. Hunt, J. N. Rawlins, The effects of hippocampal lesions upon spatial and non-spatial tests of working memory. *Behav. Brain Res.* **19**, 133–146 (1986).
16. A. D. Baddeley, G. Hitch, "Working memory" in *Psychology of Learning and Motivation*, K. Federmeier, Ed. (Elsevier, 1974), 8, pp. 47–89.
17. D. S. Olton, J. T. Becker, G. E. Handelmann, Hippocampal function: Working memory or cognitive mapping? *Physiol. Psychol.* **8**, 239–246 (1980).
18. N Solari, B Hangya, Cholinergic modulation of spatial learning, memory and navigation. *Eur. J. Neurosci.* **48**, 2199–2230 (2018).
19. B. J. Everitt, T. W. Robbins, Central cholinergic systems and cognition. *Annu. Rev. Psychol.* **48**, 649–684 (1997).
20. G. Buzsáki, Theta oscillations in the hippocampus. *Neuron* **33**, 325–340 (2002).
21. L. L. Colgin, Rhythms of the hippocampal network. *Nat. Rev. Neurosci.* **17**, 239–249 (2016).
22. H. Dannenberg *et al*., Synergy of direct and indirect cholinergic septo-hippocampal pathways coordinates firing in hippocampal networks. *J. Neurosci.* **35**, 8394–8410 (2015).
23. S. M. Montgomery, G. Buzsáki, Gamma oscillations dynamically couple hippocampal CA3 and CA1 regions during memory task performance. *Proc. Natl. Acad. Sci. U.S.A.* **104**, 14495–14500 (2007).
24. A. Fernández-Ruiz *et al*., Entorhinal-ca3 dual-input control of spike timing in the hippocampus by theta-gamma coupling. *Neuron* **93**, 1213–1226.e5 (2017).
25. M. Tamura, T. J. Spellman, A. M. Rosen, J. A. Gogos, J. A. Gordon, Hippocampal-prefrontal theta-gamma coupling during performance of a spatial working memory task. *Nat. Commun.* **8**, 2182 (2017).
26. A. G. Siapas, E. V. Lubenov, M. A. Wilson, Prefrontal phase locking to hippocampal theta oscillations. *Neuron* **46**, 141–151 (2005).
27. J. M. Fuster, G. E. Alexander, Neuron activity related to short-term memory. *Science* **173**, 652–654 (1971).
28. P. S. Goldman-Rakic, Cellular basis of working memory. *Neuron* **14**, 477–485 (1995).
29. M. Yoshida, M. E. Hasselmo, Persistent firing supported by an intrinsic cellular mechanism in a component of the head direction system. *J. Neurosci.* **29**, 4945–4952 (2009).
30. S. Funahashi, M. V. Chafee, P. S. Goldman-Rakic, Prefrontal neuronal activity in rhesus monkeys performing a delayed anti-saccade task. *Nature* **365**, 753–756 (1993).
31. M. E. Hasselmo, H. Eichenbaum, Hippocampal mechanisms for the context-dependent retrieval of episodes. *Neural Netw.* **18**, 1172–1190 (2005).
32. C. Ranganath, R. S. Blumenfeld, Doubts about double dissociations between short- and long-term memory. *Trends Cogn. Sci.* **9**, 374–380 (2005).
33. K. S. Graham, M. D. Barense, A. C. Lee, Going beyond LTM in the MTL: A synthesis of neuropsychological and neuroimaging findings on the role of the medial temporal lobe in memory and perception. *Neuropsychologia* **48**, 831–853 (2010).
34. A. Jeneson, L. R. Squire, Working memory, long-term memory, and medial temporal lobe function. *Learn. Mem.* **19**, 15–25 (2011).
35. M. Lundqvist, P. Herman, E. K. Miller, Working memory: Delay activity, yes! Persistent activity? Maybe not. *J. Neurosci.* **38**, 7013–7019 (2018).
36. C. Constantinidis *et al*., Persistent spiking activity underlies working memory. *J. Neurosci.* **38**, 7020–7028 (2018).
37. E. K. Miller, M. Lundqvist, A. M. Bastos, Working memory 2.0. *Neuron* **100**, 463–475 (2018).
38. J. E. Lisman, M. A. Idiart, Storage of 7 +/- 2 short-term memories in oscillatory subcycles. *Science* **267**, 1512–1515 (1995).
39. X. Zhou *et al*., Cholinergic modulation of working memory activity in primate prefrontal cortex. *J. Neurophysiol.* **106**, 2180–2188 (2011).
40. J. E. Lisman, O. Jensen, The θ-γ neural code. *Neuron* **77**, 1002–1016 (2013).
41. Y. Wang, S. Romani, B. Lustig, A. Leonardo, E. Pastalkova, Theta sequences are essential for internally generated hippocampal firing fields. *Nat. Neurosci.* **18**, 282–288 (2015).
42. P. Jarzebowski, C. S. Tang, O. Paulsen, Y. A. Hay, Cholinergic suppression of sharp wave-ripples impairs hippocampus-dependent spatial memory. *bioRxiv* [Preprint] (2020).
43. S. P. Jadhav, C. Kemere, P. W. German, L. M. Frank, Awake hippocampal sharp-wave ripples support spatial memory. *Science* **336**, 1454–1458 (2012).
44. A. Fernández-Ruiz *et al*., Long-duration hippocampal sharp wave ripples improve memory. *Science* **364**, 1082–1086 (2019).
45. M. Jing *et al*., An optimized acetylcholine sensor for monitoring in vivo cholinergic activity. *Nat. Methods* **17**, 1139–1146 (2020).
46. M. Vandecasteele *et al*., Optogenetic activation of septal cholinergic neurons suppresses sharp wave ripples and enhances theta oscillations in the hippocampus. *Proc. Natl. Acad. Sci. U.S.A.* **111**, 13535–13540 (2014).
47. H. Zhou *et al*., Cholinergic modulation of hippocampal calcium activity across the sleep-wake cycle. *eLife* **8**, e39777 (2019).
48. X. Ma *et al*., The firing of theta state-related septal cholinergic neurons disrupt hippocampal ripple oscillations via muscarinic receptors. *J. Neurosci.* **40**, 3591–3603 (2020).
49. C. H. Vanderwolf, Hippocampal electrical activity and voluntary movement in the rat. *Electroencephalogr. Clin. Neurophysiol.* **26**, 407–418 (1969).
50. E. F. Pace-Schott, J. A. Hobson, The neurobiology of sleep: Genetics, cellular physiology and subcortical networks. *Nat. Rev. Neurosci.* **3**, 591–605 (2002).
51. M. Lovett-Barron *et al*., Dendritic inhibition in the hippocampus supports fear learning. *Science* **343**, 857–863 (2014).
52. H. Zhang, S. C. Lin, M. A. Nicolelis, Spatiotemporal coupling between hippocampal acetylcholine release and theta oscillations in vivo. *J. Neurosci.* **30**, 13431–13440 (2010).
53. L. M. Teles-Grilo Ruivo *et al*., Coordinated acetylcholine release in prefrontal cortex and hippocampus is associated with arousal and reward on distinct timescales. *Cell Rep.* **18**, 905–917 (2017).
54. F. Marrosu *et al*., Microdialysis measurement of cortical and hippocampal acetylcholine release during sleep-wake cycle in freely moving cats. *Brain Res.* **671**, 329–332 (1995).
55. G. Buzsáki, Hippocampal sharp wave-ripple: A cognitive biomarker for episodic memory and planning. *Hippocampus* **25**, 1073–1188 (2015).
56. S. F. Owen, M. H. Liu, A. C. Kreitzer, Thermal constraints on in vivo optogenetic manipulations. *Nat. Neurosci.* **22**, 1061–1065 (2019).
57. E. Awh, E. K. Vogel, S. H. Oh, Interactions between attention and working memory. *Neuroscience* **139**, 201–208 (2006).
58. D. J. Mitchell, N. McNaughton, D. Flanagan, I. J. Kirk, Frontal-midline theta from the perspective of hippocampal "theta". *Prog. Neurobiol.* **86**, 156–185 (2008).
59. S. Raghavachari *et al*., Theta oscillations in human cortex during a working-memory task: Evidence for local generators. *J. Neurophysiol.* **95**, 1630–1638 (2006).
60. G. Buzsáki, L. W. S. Leung, C. H. Vanderwolf, Cellular bases of hippocampal EEG in the behaving rat. *Brain Res.* **287**, 139–171 (1983).
61. M. Stewart, S. E. Fox, Do septal neurons pace the hippocampal theta rhythm? *Trends Neurosci.* **13**, 163–168 (1990).
62. S. Fujisawa, A. Amarasingham, M. T. Harrison, G. Buzsáki, Behavior-dependent short-term assembly dynamics in the medial prefrontal cortex. *Nat. Neurosci.* **11**, 823–833 (2008).
63. E. Pastalkova, V. Itskov, A. Amarasingham, G. Buzsáki, Internally generated cell assembly sequences in the rat hippocampus. *Science* **321**, 1322–1327 (2008).
64. O. Jensen, J. E. Lisman, Hippocampal sequence-encoding driven by a cortical multi-item working memory buffer. *Trends Neurosci.* **28**, 67–72 (2005).
65. P. C. Petersen, G. Buzsáki, Cooling of medial septum reveals theta phase lag coordination of hippocampal cell assemblies. *Neuron* **107**, 731–744.e3 (2020).
66. S. J. Mizumori, G. M. Perez, M. C. Alvarado, C. A. Barnes, B. L. McNaughton, Reversible inactivation of the medial septum differentially affects two forms of learning in rats. *Brain Res.* **528**, 12–20 (1990).
67. Y. Norman *et al*., Hippocampal sharp-wave ripples linked to visual episodic recollection in humans. *Science* **365**, 1030 (2019).
68. A. P. Vaz, J. H. Wittig Jr, S. K. Inati, K. A. Zaghloul, Replay of cortical spiking sequences during human memory retrieval. *Science* **367**, 1131–1134 (2020).
69. Y. Liu, R. J. Dolan, Z. Kurth-Nelson, T. E. J. Behrens, Human replay spontaneously reorganizes experience. *Cell* **178**, 640–652.e14 (2019).
70. S. Gais, J. Born, Low acetylcholine during slow-wave sleep is critical for declarative memory consolidation. *Proc. Natl. Acad. Sci. U.S.A.* **101**, 2140–2144 (2004).
71. E. Esposito *et al*., Potential circadian effects on translational failure for neuroprotection. *Nature* **582**, 395–398 (2020).